Automated Hierarchical Time Gain Compensation for In Vivo Ultrasound Imaging

Moshavegh, Ramin; Hemmsen, Martin Christian; Martins, Bo; Brandt, Andreas Hjelm; Lindskov Hansen, Kristoffer; Nielsen, Michael Bachmann; Jensen, Jørgen Arendt

Published in:
Proceedings of SPIE

Link to article, DOI:
10.1117/12.2081619

Publication date:
2015

Paper presented at the SPIE Medical Imaging 2015 Conference:

Automated Hierarchical Time Gain Compensation for *In Vivo* Ultrasound Imaging

Ramin Moshavegh, Martin Christian Hemmsen, Bo Martins, Andreas Hjelm Brandt, Kristoffer Lindskov Hansen, Michael Bachmann Nielsen and Jørgen Arendt Jensen

Center for Fast Ultrasound Imaging,
Biomedical Engineering Group,
Department of Electrical Engineering
Ørsteds Plads Building 349,
Technical University of Denmark,
2800 Kgs. Lyngby, Denmark.

To be published in the Proceedings of SPIE Medical Imaging 2015.

Automated Hierarchical Time Gain Compensation for *In Vivo* Ultrasound Imaging

Ramin Moshavegh[a], Martin Christian Hemmsen[a], Bo Martins[b],Andreas Hjelm Brandt[c], Kristoffer Lindskov Hansen[c], Michael Bachmann Nielsen[c] and Jørgen Arendt Jensen[a]

[a]Center for Fast Ultrasound Imaging, Department of Electrical Engineering, Technical University of Denmark, DK-2800 Lyngby, Denmark
[b]BK Medical ApS, Herlev, Denmark
[c]Department of Radiology, Copenhagen University Hospital, Copenhagen, Denmark

ABSTRACT

Time gain compensation (TGC) is essential to ensure the optimal image quality of the clinical ultrasound scans. When large fluid collections are present within the scan plane, the attenuation distribution is changed drastically and TGC compensation becomes challenging. This paper presents an automated hierarchical TGC (AHTGC) algorithm that accurately adapts to the large attenuation variation between different types of tissues and structures. The algorithm relies on estimates of tissue attenuation, scattering strength, and noise level to gain a more quantitative understanding of the underlying tissue and the ultrasound signal strength. The proposed algorithm was applied to a set of 44 *in vivo* abdominal movie sequences each containing 15 frames. Matching pairs of *in vivo* sequences, unprocessed and processed with the proposed AHTGC were visualized side by side and evaluated by two radiologists in terms of image quality. Wilcoxon signed-rank test was used to evaluate whether radiologists preferred the processed sequences or the unprocessed data. The results indicate that the average visual analogue scale (VAS) is positive (p-value: 2.34×10^{-13}) and estimated to be 1.01 (95% CI: 0.85; 1.16) favoring the processed data with the proposed AHTGC algorithm.

Keywords: Time gain compensation, Attenuation estimation, Attenuation variation, Signal-to-noise ratio, Ultrasound imaging

1. INTRODUCTION

Radiofrequency (RF) echoes are strongly attenuated by the tissues scanned.[1] These RF signals span a wide dynamic range, when they are received by the transducer, and are not suitable to be visualized before the gains are adjusted. Time gain compensation (TGC) is usually utilized to compensate for the acoustic attenuation. TGC offsets the attenuation of ultrasound echo signals along the depth, so that echoes belonging to deep structures are more amplified compared to superficial echoes. This provides more uniform image to be displayed on the scanner.[1]

Current ultrasound scanners use a TGC curve for time gain compensation. The user adjusts the shape by manually using TGC sliders for different depths. However, this is cumbersome and the image quality is highly dependent on the adjustments. An automatic adjustment of the TGC (ATGC) without user intervention can address the shortcomings of the manual TGC.[2] To date, several designs of ATGC are proposed in the literature.[1–3] However, the majority of these algorithms rely on the presence of sufficiently large homogeneous soft tissues with an uniform distribution of attenuation.[1,3,4] In other words, the dependency of the attenuation for several different tissues is ignored in these algorithms. These methods fail to compensate the overall gain when large fluid collections such as the urine bladder or gallbladder exist that change the uniform distribution of the attenuation drastically. Large anechoic segments, surrounded by soft tissue, present a large variation in attenuation.

This paper extends the adaptive ATGC algorithm developed by Hemmsen et al.,[5] and propose an automated hierarchical TGC (AHTGC) algorithm with focus on images with large anechoic regions. The algorithm is based on a physical understanding of the underlying tissue based on the scattering strength, signal-to-noise ratio,

Further author information: Ramin Moshavegh, E-mail: ramosh@elektro.dtu.dk

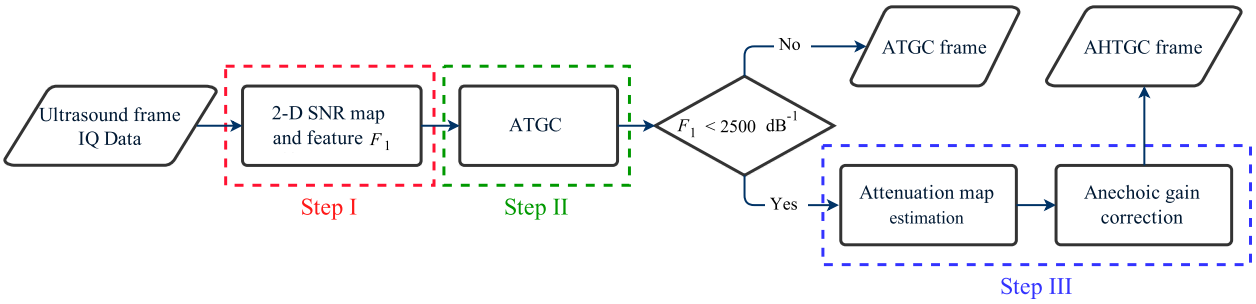

Step I: A 2-D SNR map for each frame is computed and the slope at 80th percentile of its cumulative histogram (i.e. feature F_1) is determined.
Step II: A TGC curve is automatically determined for each frame and used to compensate the gains in that frame. the input to this step is the envelope of RF-data. The output of this step is called ATGC frame.
Step III: A normalized 2-D attenuation map is generated for scans with large fluid collections, and used to correct the gains inside the fluid regions. The input to this step is the RF-data, and the output of this step is called AHTGC frame.

Figure 1: Block diagram of the AHTGC algorithm.

focusing gain, and tissue attenuation. From these, different constituents of the tissue can be determined. For this purpose, the decay of the power spectrum frequency components of the received signal with respect to depth is considered to estimate the attenuation and to adapt the ATGC to the large attenuation variations. The remainder of this paper is organized as follows. Section 2 introduces the proposed algorithm. Section 3 presents the *in vivo* results of the proposed AHTGC algorithm and discusses the findings. Finally section 4 is the conclusion and the perspectives.

2. MATERIALS AND METHODS

It is common practice to assume that the attenuation has a linear relation with the frequency of the acoustic wave.[6] In this paper, the spectral difference method adapted from Kuc[6] is used to generate 2-D attenuation maps. These maps are then used to correct the mis-adjusted gains by the ATGC algorithm inside the anechoic regions.

The proposed algorithm contains three distinct steps. First, a 2-D signal-to-noise ratio (SNR) map for each frame is computed. Based on the SNR map it was decided if the frame contained large anechoic regions or not. Then, a TGC curve is computed using the algorithm of Hemmsen et al.[5] This TGC curve is applied to the original ultrasound frame. A 2-D attenuation map is then generated from the original image and is used to correct the adjusted gains inside the anechoic regions after applying the TGC curve. This correction is done only on the scans including large fluid regions. The block diagram of the proposed AHTGC is shown in the Fig. 1. Three main steps of the algorithm are shown on the diagram and discussed in detail in this section.

2.1 Step I. SNR map computation

Complex IQ data is used to compute the signal to noise ratio (SNR) for all the frames. The acquired frame from the transducer, is contaminated with noise and can be written as

$$\mathbf{Y}_i = \mathbf{S}_i + \mathbf{E}_i \tag{1}$$

where matrix $\mathbf{S}_i$ is the desired frame signal, $\mathbf{E}_i$ is the noise contribution, and i is the frame number. The measurement is performed on a tissue mimicking phantom with an attenuation of 0.5 dB/cm $\times$ MHz and N frames acquired, the mean acquired signal is given by

$$\mathbf{M} = \hat{\mathbf{Y}} = E\{\mathbf{Y}_i\} = E\{\mathbf{S}_i + \mathbf{E}_i\} = \frac{1}{N}\sum_{i=1}^{N}(\mathbf{S}_i + \mathbf{E}_i) \tag{2}$$

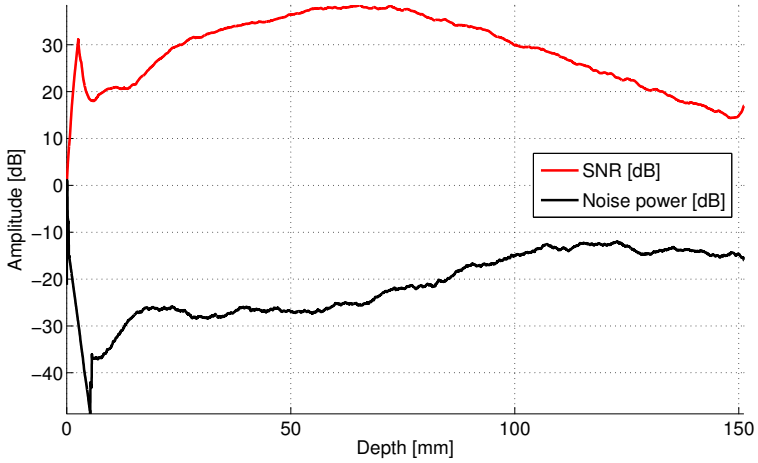

Figure 2: SNR and noise contribution belonging to the center line of scan of a tissue mimicking phantom with an attenuation of 0.5 dB/cm × MHz.

in which matrix $\mathbf{M}$ represents the mean of acquired frames. Also given the assumption that $E\{\mathbf{E}_i\} = 0$, the mean acquired signal by averaging all the frames will be equivalent to the mean desired signal and can be written as

$$\mathbf{M} = \hat{\mathbf{Y}} = \hat{\mathbf{S}} \tag{3}$$

The noise contribution for each frame is estimated by subtracting the mean of the all frames from a single frame

$$\mathbf{E}_i = \mathbf{Y}_i - \hat{\mathbf{Y}} \tag{4}$$

Therefore, The noise power for the ultrasound device is expressed as follows:

$$\mathbf{P}_{noise} = \left| \frac{1}{N} \sum_{i=1}^{N} \mathbf{E}_i^2 \right| \tag{5}$$

Finally, the SNR map for an acquired *in vivo* frame is determined by dividing the signal power of that frame by the system noise power computed from (5)

$$\mathbf{P}_{signal}(i) = |\mathbf{Y}_i|^2 \tag{6}$$

$$\mathbf{SNR}_{dB}(i) = 10 \log_{10} \left(\frac{\mathbf{P}_{signal}(i)}{\mathbf{P}_{noise}} \right) \tag{7}$$

where $\mathbf{Y}_i$ in (6) is the signal acquired from frame number i in a sequence of *in vivo* scans. The power of signal changes from frame to frame, while the noise power is unchanged. The variation of noise and SNR with depth for a scan of tissue mimicking phantom along its center line is depicted in Fig. 2. Also two examples of the 2-D SNR maps computed from scans of the human bladder and liver are shown in Figs. 3a and 3c respectively. The essential first step in the proposed time gain compensation algorithm was to determine whether the scans included large fluid collections or not. As it is anticipated, fluid collections appear as very low SNR regions in the SNR maps. A feature is specifically designed to characterise this property in SNR maps. First, cumulative histogram of the values inside the SNR map is computed. Then, a curve is fitted to the counts and the slope of the fitted curve at 25th and 80th percentiles of the curve was used to characterise the amount of fluid in the scans.

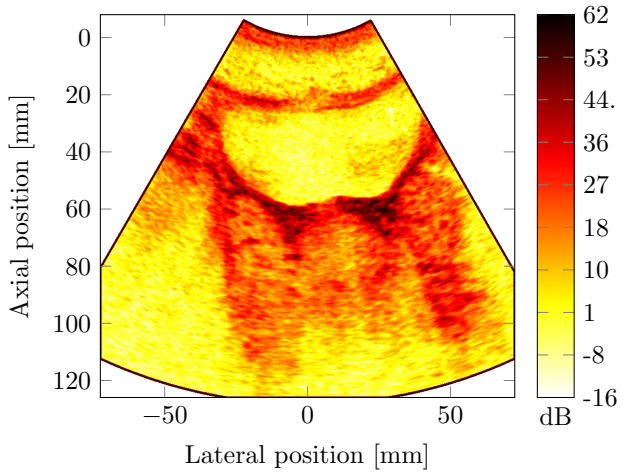

(a) 2-D SNR map calculated from scan of human bladder.

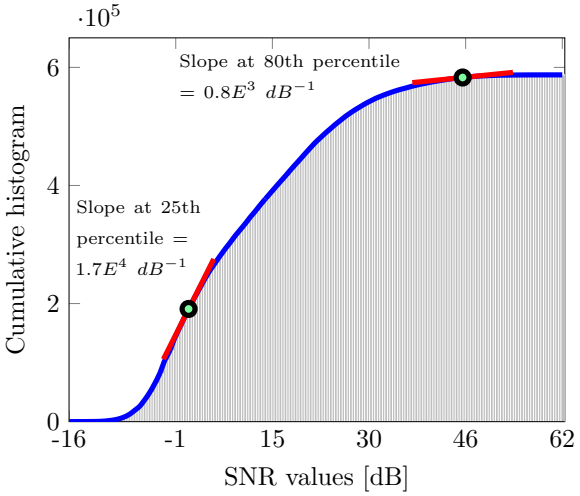

(b) Cumulative histogram of SNR values in map *(a)*.

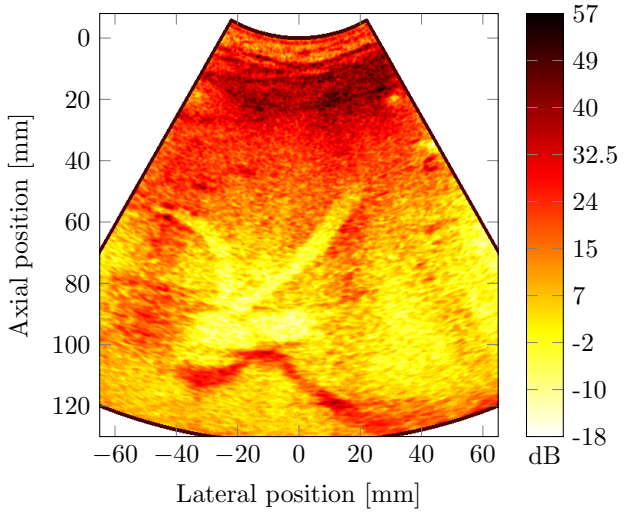

(c) 2-D SNR map calculated from scan of human liver.

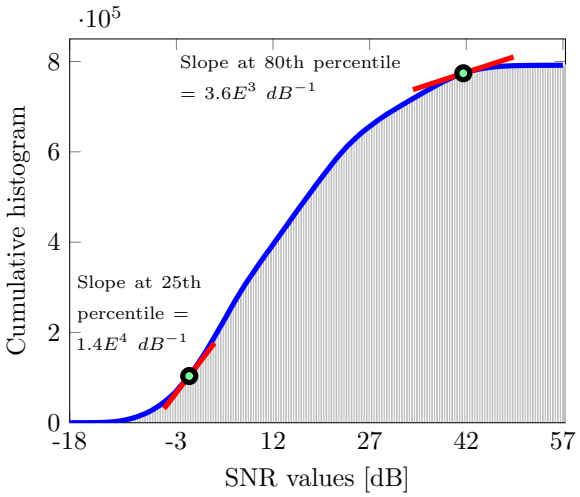

(d) Cumulative histogram of SNR values in map *(c)*.

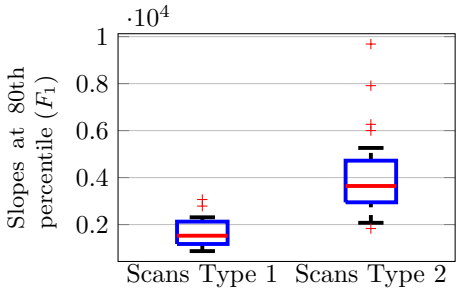

Type 1: Scans with large fluid regions.
Type 2: Scans with small or no fluid regions.

(e) Distribution of 80th percentile slopes (feature F_1)for two types of scans.

Figure 3: Two examples of 2-D SNR maps computed for scans of human bladder and liver with illustration of how their corresponding slope feature is calculated. (a) 2-D SNR map of the human bladder. (b) Cumulative histogram of all SNR values in map *(a)* and slopes calculated at 25th and 80th percentiles of the fitted curve. (c) 2-D SNR map of the human liver. (d) Cumulative histogram of the values in map *(c)* and slopes calculated at 25th and 80th percentiles of the fitted curve. (e) Boxplots of 80th percentile slopes for two types of scans.

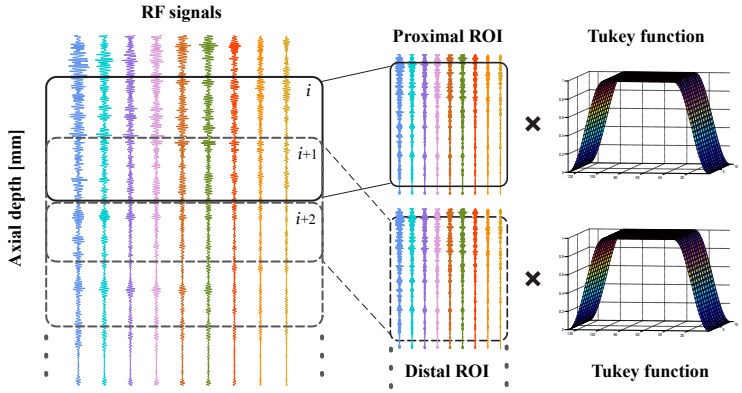

Figure 4: Illustration of how RF data is subdivided into sets of different proximal and distal windows.

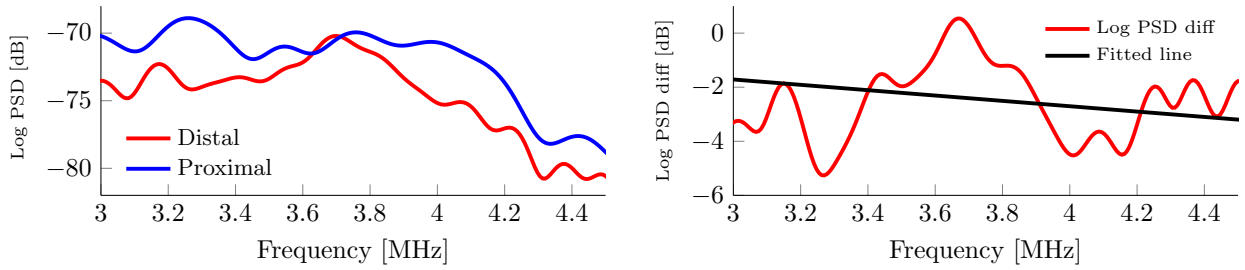

(a) Example Log PSD of a paired proximal and distal segments, where the $f_0 = 3.75$ MHz.

(b) Log PSD difference, and fitted line with slope $= -0.502$ dB/cm $\times$ MHz.

Figure 5: Illustration of how the attenuation value for a pair of proximal and distal segments is computed.

The idea behind using these two features was to benefit from changes in distribution of SNR values in SNR maps to distinguish between different scans. Number of counts of low SNR values in scans with large fluid collections is higher compared to that of scans with small or no fluid collections. This yielded a bigger slope of cumulative histogram at low SNR values (i.e. 25th percentile) for scans with large anechoic regions compare to that of scans with no anechoic regions. The same effect decreased the slope of cumulative histogram at high SNR values (i.e. 80th percentile) for scans with large anechoic regions compared to that of scans with no anechoic regions. The rate of decrease in the slope at 80th percentile is much bigger than the increase in the slope at 25 percentile. Therefore, it was decided to use the slope at 80th percentile (F_1) to distinguish between the two different scans with large fluid collections and small or no fluid collections. The value of F_1 was determined empirically using 4 scans additional to the 44 scans used for evaluation of the AHTGC algorithm. $F_1 < 2500$ dB^{-1} characterised a scan with large fluid collection, otherwise, the scan was considered to contain small or no collections of fluid.

Figures 3b and 3d illustrate how this feature is calculated for two scans of the human bladder and liver. These two figures show the cumulative histogram of the SNR images over 100 bins. 100 bins are used to ensure that high variation of SNR values in each map is captured in the histogram and also precision of the density estimation is not jeopardized. In the next step of the algorithm, each scan is dynamically compensated for the attenuated gain using a TGC curve.

2.2 Step II. TGC compensation by ATGC

Gains were corrected for all depths for each frame to obtain homogeneous images. The automatic TGC correction in this section simulated the TGC adjustments performed by a physician, eliminating the possible mistakes due to user intervention.[5] The algorithm used envelope of RF-data as input. The correction was performed by calculating a mask to filter out strong and weak specular regions inside the envelope data. The mask was

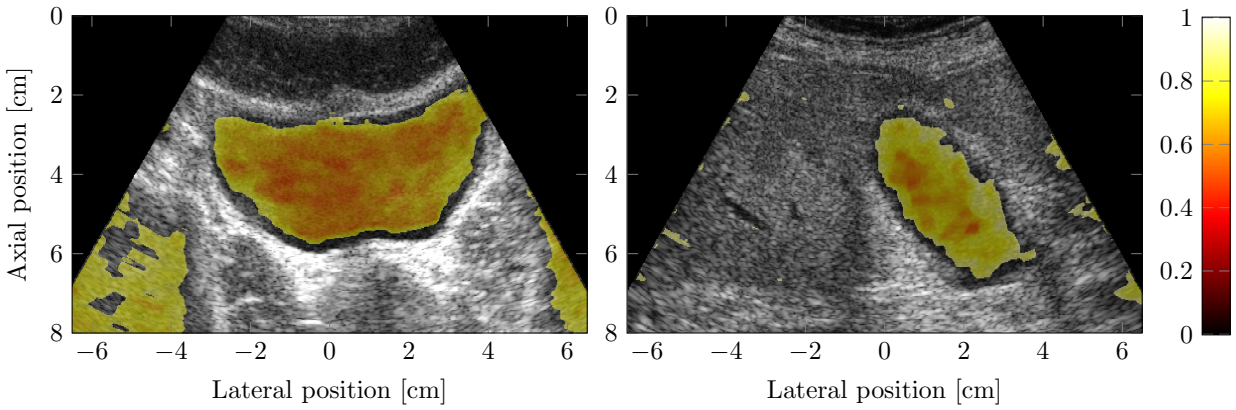

(a) Normalized attenuation map of a human bladder. (b) Normalized attenuation map of a scan of human gallbladder.

Figure 6: Examples of normalized attenuation maps overlaying on B-mode images

then applied to each envelope detected data and the median value of all scan-lines for all depths in the recorded frame was found. The resulting curve was normalized to a maximum of one, inverted and used to normalize all scan-lines in that frame. The compensation is finally performed by dividing the values in every column by the TGC curve. Next step of the proposed hierarchical algorithm is to compute 2-D attenuation maps for those scans including large fluid collections. This is done by using a spectral difference method described in the next section.

2.3 Step III. Attenuation map estimation and gain correction

An attenuation map is calculated for those scans characterised to have large fluid regions in step I. This map is used to correct the over-gained regions inside the fluid collections after they compensated with a the TGC curve in step II.

Beamformed RF data was used to compute the attenuation maps. Each RF line was partitioned into several overlapping segments, in which each RF segment was gated axially by a Tukey window to alleviate the spectral leakage at both boundaries. Each two overlapping segments in the RF line were paired together, where the upper segment was considered as proximal and the underlying segment was considered as distal segment. For each pair the difference between the logarithm of power spectra computed, a line fitted to the power spectral difference, and the slope of the resulting line considered as an attenuation value for the proximal segment (see Fig. 5). Both proximal and distal segments were moved down on the RF line and several attenuation values were calculated along the RF line by pairing the proximal and distal segments. Blocks were overlapped by 50% to increase axial resolution of the attenuation maps. Figure 4 shows how the RF data is subdivided into pairs of proximal and distal windows and overlapped to increase the axial and lateral resolutions. The resulted attenuation values for RF lines are laterally averaged over scan lines to reduce the high variability of the attenuation values in the map.

Figure 6 shows examples of computed and normalized attenuation maps overlaying on B-mode images. The length of the RF segments and the number of averaging scan lines determine the axial and lateral resolution of the estimated attenuation maps respectively. Literature suggests the axial RF segment lengths to be between 1 to 2 cm.[7] It also suggests that the number of the averaging lines should be between 8 to 25 RF lines. In this study, anechoic regions adjacent to soft tissues presented large attenuation variation. To capture this variation, the length of axial segments was set to 1 cm, and the number of averaging RF lines was set to 10 lines. The generated attenuation maps were then normalized and multiplied to the compensated images by ATGC,[5] to correct the gains inside the anechoic regions.

3. RESULTS AND DISCUSSION

The proposed AHTGC algorithm was applied to *in vivo* abdominal scans. Fifteen subjects were scanned and a total of 44 abdominal sequences each containing 15 frames were acquired. In addition to the urine bladder

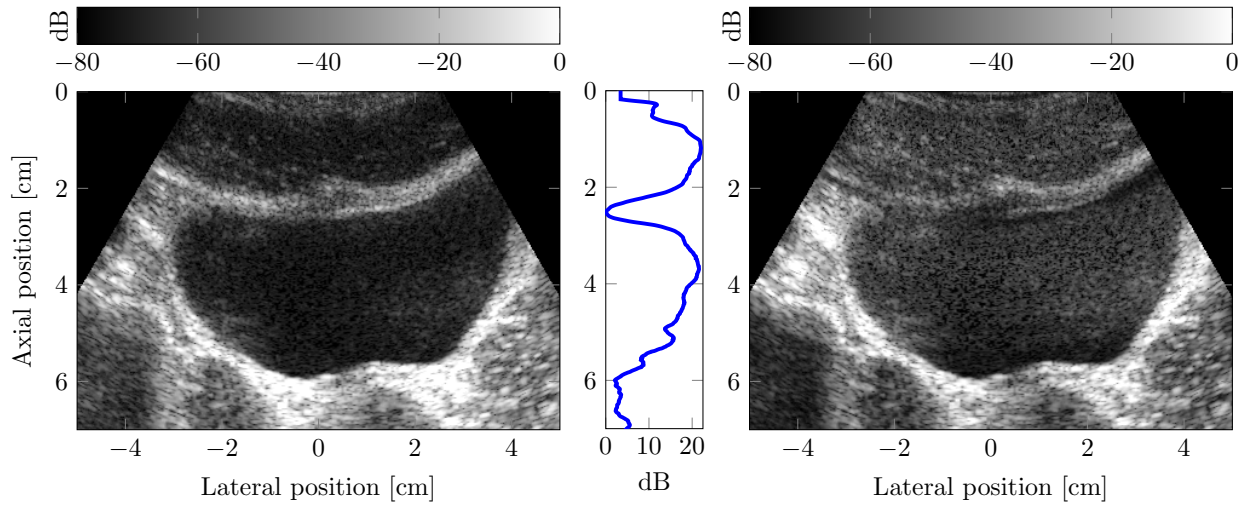

(a) Un-processed axial scan of human bladder. (b) TGC (c) ATGC compensated Image *(a)* with curve *(b)*.

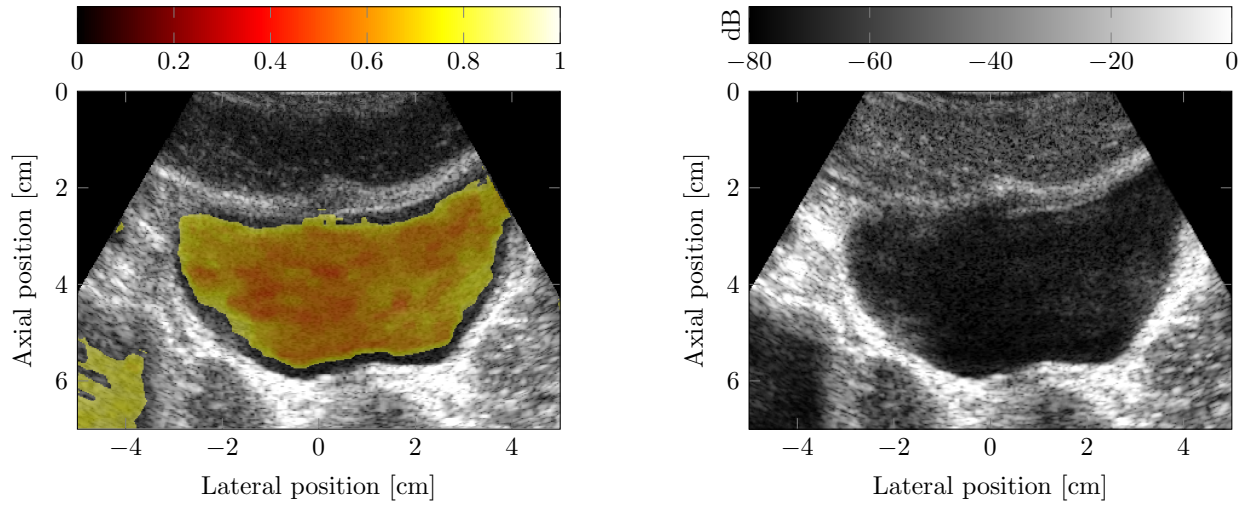

(d) Normalized attenuation map computed from image *(a)*. (e) AHTGC corrected image *(c)* with 2-D map *(d)*.

Figure 7: Illustration of how the proposed AHTGC algorithm is applied to a axial scan of the human bladder. (a) Un-processesed scan. (b) TGC curve computed by the ATGC method in section 2.2. (c) ATGC compensated image *(a)* with curve *(b)*. (d) 2-D attenuation map computed from image *(a)*. (e) Attenuation corrected image *(c)* with map *(d)*.

and gallbladder scans that have large anechoic regions, other anatomical locations such as the liver and kidney were also included in the dataset. This was done to evaluate the performance of the algorithm on images with less-variable attenuation distribution. The beamformed RF data were acquired using a 2202 ProFocus ultrasound scanner (BK Medical, Denmark) connected to a 192-element 3.5 MHz convex array transducer (8820e, BK Medical). The dynamic received focus technique with factory preset TGC was employed to generate the sequences. A research interface connected to the scanner simultaneously recorded the real-time beamformed RF data from the scanner.[8]

The proposed AHTGC algorithm was applied to the acquired image sequences off-line in Matlab(2013b). Figure 7 shows an example of the experimental results of the AHTGC algorithm applied to a axial scan of the human bladder. The figure illustrates how the gains were first compensated by ATGC, and then corrected using

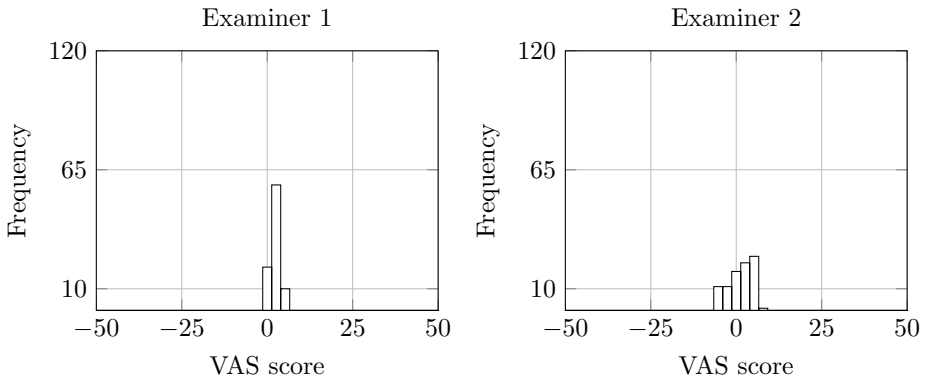

Figure 8: Distribution of pooled answers from assessment of overall image quality by two expert radiologists. Positive values favor AHTGC algorithm.

a 2-D attenuation profile. Figure 7a shows the original image in which gains were only adjusted by the factory preset TGC with no default gains. Figure 7b shows the calculated TGC curve using the ATGC method discussed in the Section 2.2. Figure 7c shows the the compensated image using the ATGC. Whilst the resulting image is more homogeneous, the area inside the bladder is highly over-gained. The normalized 2-D attenuation profile (see Fig. 7d) computed using the method introduced in Section 2.3 was then multiplied with the ATGC compensated image to correct the mis-adjusted high gains inside the bladder. The result is shown in the Fig. 7e. It can be observed that inside of the bladder is not over-gained and the uniformity of the result is comparable to the ATGC corrected image shown in Fig. 7c.

A double blinded study was conducted to evaluate the performance of the AHTGC algorithm. Matching pairs of *in vivo* sequences, unprocessed and processed with AHTGC, were evaluated side by side by two experienced radiologists. Each pair was shown twice by randomizing the left and right positioning. This yielded a total of 176 independent visual evaluations. The radiologists were then asked to score the image quality of each pair on a visual analogue scale (VAS) ranging between -50 and +50. This is performed by dragging a slider towards their favored movie sequence, where a positive scale favors the processed sequence with the AHTGC algorithm. The distribution of ratings from the individual doctors are shown in Fig. 8. Wilcoxon signed-rank test was applied to assess whether radiologists preferred the processed sequences or the unprocessed data. The computed average VAS score is positive (p-value: 2.34×10^{-13}) and estimated to be 1.01 (95% CI: 0.85; 1.16) favoring the compensated data with the AHTGC algorithm. Although the average VAS scores is not significantly positive, doctors consistently chose the processed images with AHTGC to be better than the unprocessed images.

A secondary evaluation was conducted to assess the discrimination power of the feature F_1 to differentiate between two types of the scans. 44 scans used in this study were visually divided into two categories, 11 scans including large fluid collections (type 1) and 33 scans with small or no collections of fluid (type 2). Feature F_1 was computed for all scans and boxplots illustrating the distribution of F_1 for two types of scans were generated and shown in Fig. 3e. No overlap between interquartile interval of the two boxplots indicated that feature F_1 was able to discriminate between two types of scans.

4. CONCLUSION

This paper presented a hierarchical ATGC (AHTGC) algorithm, where estimates of SNR and attenuation profiles used to correct the gains after applying the ATGC. The new algorithm presents a robust and more flexible control over gain especially inside the large anechoic regions. In addition, the proposed method adjusts the gains automatically, which increases the clinical throughput by avoiding unnecessary user manual adjustments of TGC on the scanner. Furthermore, the 2-D attenuation profiles provide solid foundation for other processes like segmentation of the tissues and structures.

ACKNOWLEDGMENTS

This work was financially supported by grant 82-2012-4 from the Danish Advanced Technology Foundation and from BK Medical ApS, Herlev, Denmark.

REFERENCES

[1] Lee, D., Kim, Y. S., and Ra, J. B., "Automatic time gain compensation and dynamic range control in ultrasound imaging systems," *Proc. SPIE Med. Imag.* **6147**, 614708–614708–9 (2006).

[2] Pye, S., Wild, S., and McDicken, W., "Adaptive time gain compensation for ultrasonic imaging," *Ultrasound Med. Biol.* **18**(2), 205–212 (1992).

[3] Tang, M., Luo, F., and Liu, D., "Automatic time gain compensation in ultrasound imaging system," *Proc. IEEE Int. Conf. Bioinfo. Biomed. Eng.* , 1–4 (2009).

[4] Klesenski, K., "Automatic gain compensation in an ultrasound imaging system," *US Patent* , 5,579,768 (1996).

[5] Hemmsen, M. C., Hansen, P. M., Lange, T., Hansen, J. M., Hansen, K. L., Nielsen, M. B., and Jensen, J. A., "In vivo evaluation of synthetic aperture sequential beamforming," *Ultrasound Med. Biol.* **38**(4), 708–716 (2012).

[6] Kuc, R., "Estimating acoustic attenuation from reflected ultrasound signals: Comparison of spectral-shift and spectral-difference approaches," *IEEE Trans. Acous., Speech, Sig. Pro.* **32**(1), 1–6 (1984).

[7] Klimonda, Z., Litniewski, J., and Nowicki, A., "Spatial resolution of attenuation imaging," *Archives of Acoustics* **34**(4), 461–470 (2009).

[8] Hemmsen, M. C., Nikolov, S. I., Pedersen, M. M., Pihl, M. J., Enevoldsen, M. S., Hansen, J. M., and Jensen, J. A., "Implementation of a versatile research data acquisition system using a commercially available medical ultrasound scanner," *IEEE Trans. Ultrason., Ferroelec., Freq. Contr.* **59**(7), 1487–1499 (2012).